

# Performances of a GEM-based Time Projection Chamber prototype for the AMADEUS experiment

---

**M. Poli Lener<sup>a\*</sup>, M. Bazzi<sup>a</sup>, G. Corradi<sup>a</sup>, C. Curceanu<sup>a</sup>, A. D'Uffizi<sup>a</sup>, C. Paglia<sup>a</sup>,  
A. Romero Vidal<sup>a b</sup>, E. Sbardella<sup>a</sup>, A. Scordo<sup>a</sup>, D. Tagnani<sup>a</sup>, J. Zmeskal<sup>c</sup>**

<sup>a</sup>*Laboratori Nazionali di Frascati -INFN,  
Frascati, Italy*

<sup>b</sup>*Universidad de Santiago de Compostela,  
Santiago de Compostela, Spain*

<sup>c</sup>*Stefan Meyer Institut für subatomare Physik,  
Vienna, Austria*

*E-mail: marco.polilener@lnf.infn.it*

**ABSTRACT:** A large number of high-energy and heavy-ion experiments successfully used Time Projection Chamber (TPC) as central tracker and particle identification detector. However, the performance requirements on TPC for new high-rate particle experiments greatly exceed the abilities of traditional TPC read out by multi-wire proportional chamber (MWPC). Gas Electron Multiplier (GEM) detector has great potential to improve TPC performances when used as amplification device.

In this paper we present the R&D activity on a new GEM-based TPC detector built as a prototype for the inner part for AMADEUS, a new experimental proposal at the DAΦNE collider at Laboratori Nazionali di Frascati (INFN), aiming to perform measurements of the low-energy negative kaons interactions in nuclei.

In order to evaluate the GEM-TPC performances, a 10x10 cm<sup>2</sup> prototype with a drift gap up to 15 cm has been realized. The detector was tested at the  $\pi$ M1 beam facility of the Paul Scherrer Institut (PSI) with low momentum pions and protons, without magnetic field. Drift properties of argon-isobutane gas mixtures are measured and compared with Magboltz prediction. Detection efficiency and spatial resolution as a function of a large number of parameters, such as the gas gain, the drift field, the front-end electronic threshold and particle momentum, are illustrated and discussed. Particle identification capability and the measurement of the energy resolution in isobutane-based gas mixture are also reported.

**KEYWORDS:** Micro-Pattern Gas Detectors ; TPC; Tracking detectors; Particle Identification Detectors.

---

\*Corresponding author.



---

## Contents

<b>1. Introduction</b>	<b>1</b>
<b>2. AMADEUS TPG prototype production</b>	<b>2</b>
<b>3. Experimental test setup and data taking</b>	<b>4</b>
3.1 The readout electronics	5
<b>4. Gas Mixture Choice</b>	<b>6</b>
4.1 Primary Ionization	6
4.2 Gas Gain Measurement	7
<b>5. Detector Performances</b>	<b>7</b>
5.1 Drift Velocity	7
5.2 Efficiency	9
5.3 Spatial Resolution	11
5.4 Time Over Threshold measurement	13
5.5 Particle Identification using $dE/dx$	14
5.6 Edge Effect due to the Field Cage	15
<b>6. Conclusion</b>	<b>17</b>

---

## 1. Introduction

The AMADEUS experiment [1],[2] aims to perform measurements of low-energy charged kaons interaction in nuclear matter, in particular to search for the so-called “kaonic nuclear clusters”. The AMADEUS setup is going to be installed inside the KLOE detector [3] in the free space inside the drift chamber (Fig. 1). The experiment will then use the drift chamber (DC) and the calorimeter of the KLOE detector, together with a dedicated setup consisting of a target cell to be filled with deuterium or helium (3 and 4), a trigger system, which will trigger on the back-to-back  $K^+ K^-$  pairs emitted from the decay of the  $\Phi$  particles produced at the DAΦNE  $e^+ e^-$  collider of the LNF-INFN [4],[5],[6] and an inner tracker, namely a Time Projection Chamber, TPC, equipped with Gas Electron Multiplier [7] (Fig. 2).

The GEM-based TPC (TPG) will be 20 cm long with an inner diameter of 8 cm and an outer one of 40 cm.

The required performances for the TPG AMADEUS are: a spatial resolution better than  $200 \mu\text{m}$  in X-Y and  $300 \mu\text{m}$  in Z in order to achieve together with the KLOE DC a momentum resolution better than 1% in a magnetic field of 0.5 T; a detector material budget lower than 0.5% of  $X_0$ ; a



rate capability of  $\sim 1 \text{ kHz/cm}^2$  [9]. In addition, the detector must operate in continuous mode, which means an ion feedback below  $10^{-3}$  [10], and it must tolerate, without performance losses, an integrated charge of  $\sim 0.05 \text{ C/cm}^2$  in 1 year of operation at a gas gain of 6000 and an average particle flux of  $1 \text{ kHz/cm}^2$  [11].

Since most of the above requirements are easily fulfilled by a TPG, the R&D activity at the Laboratori Nazionali di Frascati (INFN) is mainly focused on the choice of the gas mixture, in order to achieve the highest spatial resolution with a 0.5 T value of magnetic field, and on the design of the detector readout.

A prototype of the AMADEUS TPG detector was built and tested both in laboratory and at Paul Scherrer Institut (PSI). The technique used in the prototype construction is described in Sec. 2, while the experimental setup is briefly reported in Sec. 3. The choice of the gas mixtures is described in Sec. 4 together with the estimate of the primary ionization and the measurement of the gas gain. In Sec. 5 the overall detector performances obtained at the PSI, in terms of detection efficiency, spatial resolution, PID capability and energy resolution, are presented and discussed. The paper ends with the conclusions.

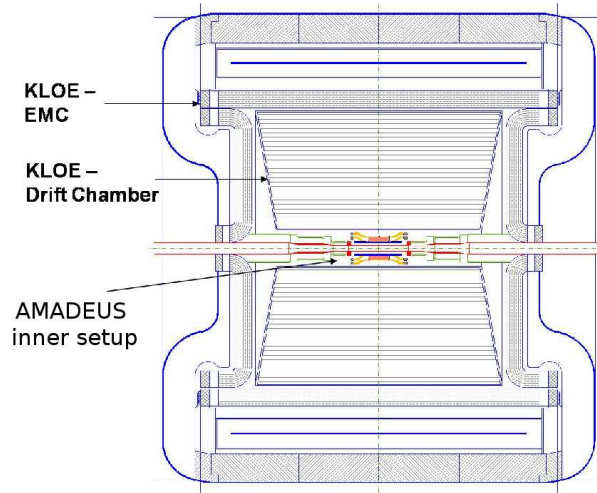


**Figure 1.** Cross-section of the KLOE detector including the AMADEUS inner setup inside the Drift Chamber.

## 2. AMADEUS TPG prototype production

The TPG prototype construction has been performed in a class 1000 clean room. The detector is composed by three GEM foils glued on Fiberglass (FR4) frames, defining the gaps between GEM themselves, then sandwiched between a cathode and anode PCBs. The exploded view of the detector is shown in Fig. 3.

The GEM foils, manufactured by CERN-EST-DEM workshop, have an active area of  $10 \times 10 \text{ cm}^2$ . Severe criteria have been adopted for GEM foils acceptance: the defects, detected by means of microscope inspection, must have an area smaller than  $1 \text{ mm}^2$ ; a maximum leakage current of 1 nA at 600 V, measured with a residual humidity of about 20%, is required.



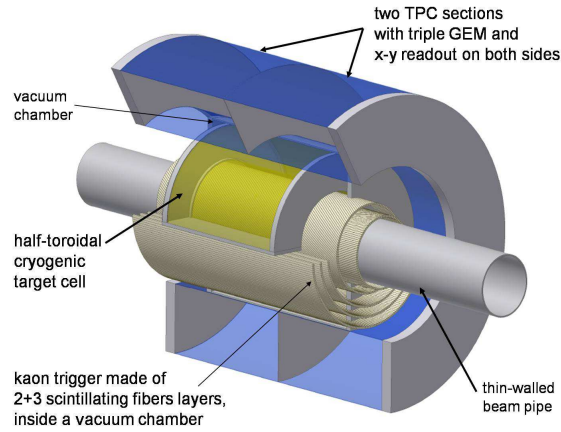


**Figure 2.** The inner setup of AMADEUS. From the beam pipe to the outer region: the Kaonic Trigger, the Gas Target and the TPG.

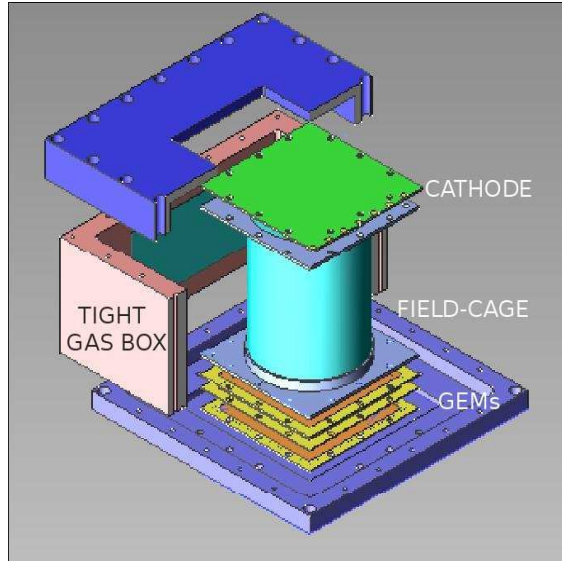


**Figure 3.** Exploded view of the GEM-based TPC detector.

To ensure high stability of detector operation without requiring a grid spacer inside the active area, a stretching technique of the GEM foil before the frame gluing has been used [8]. This technique was developed for the R&D of the GEM for the LHCb Muon Chamber. In Fig. 4 the home-made tool used for the production is shown.

In Ref. [9] the extensive campaign of measurements is reported, such as the maximum sag due to electrostatic forces between GEMs, the kapton creep and radiation effects, which have been performed in order to avoid electrostatic instability and to achieve a good uniformity response.

The electric field uniformity in the drift volume is provided by a cylindrical field cage, which consists of two sets of copper strips (2.5 mm wide) on both sides of an insulating Kapton foil (15 cm height), where the outer strips cover the gaps between the inner strips. The potential on each ring is defined by a precision resistor chain located outside the gas volume. The cylindrical shape



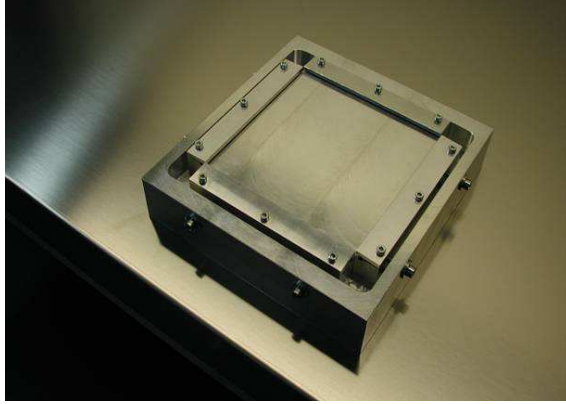


**Figure 4.** Picture of the home-made tool used for stretching the GEMs before the frame gluing. A mechanical tension of  $1 \text{ kg/cm}^2$  is applied on the edges of the foil.

has been obtained by exploiting the vacuum bag technique [12] and rolling the copper-kapton foil onto machined Polytetrafluorethylene (PTFE) cylinders that act as molds (Fig. 5). The edges of the foil are glued together with bi-component epoxy along the axial millimetric overlap (2–3 mm wide). After the curing cycle, the field-cage foil is easily removed from the cylindrical mold: the results is a perfectly cylindrical field-cage. To ensure a mechanical support, two fiberglass flanges are glued on the edges with Araldite 2011.

In this R&D phase, the detector has been encapsulated inside a tight gas box which has been provided by two  $14 \times 12 \text{ cm}^2$  windows, covered by  $10 \text{ }\mu\text{m}$  Mylar film, in order to reduce as much as possible the radiation length for a particle crossing the detector (Fig. 6). The gas tightness of the detector has been measured and it is lower than 2 mbar per day, corresponding to less than 100 ppmV of residual humidity with a gas flux of 100 cc/min.



**Figure 5.** A cylindrical field-cage foil realised with vacuum bag technique.

### 3. Experimental test setup and data taking

The performance of the TPG prototype has been studied at the  $\pi\text{M1}$  beam facility of the Paul Scherrer Institut (PSI) without magnetic field. The  $\pi\text{M1}$  beam is a quasi-continuous high-intensity secondary beam providing pions or protons with very precise momentum resolution.



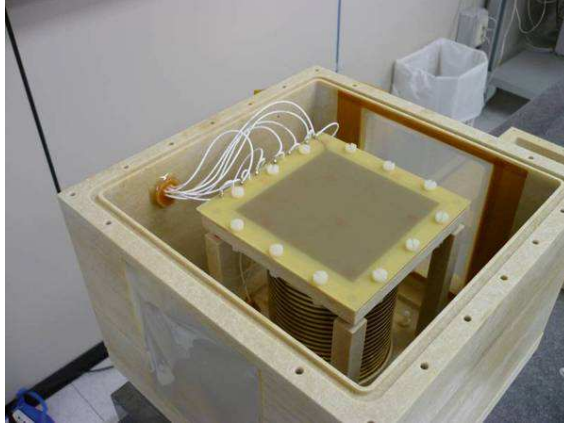


**Figure 6.** Tight gas box for the TPG. The two windows used for the particle crossing the detector and the HV connections of the various electrodes are visible.

The study of the detection efficiency, spatial and energy resolution of the detector has been performed with a beam rate of  $\sim 200$  Hz.

The trigger consisted of the coincidence of three scintillators  $S1 \otimes S3 \otimes S2$ , centered on the beam axis. The distance between the two scintillators  $S1 \otimes S3$  and the  $S2$  scintillator was about 20 cm as shown in Fig. 7. The area covered by the intersection of these 3 scintillators is approximately  $12 \times 20 \text{ mm}^2$ .

The horizontal size (12 mm) of  $S1$  and  $S2$  was chosen in order to completely cover the width of the detector readout as described in the following section, while the 20 mm width of the  $S3$  scintillator was used in order to limit the vertical size of the beam. Such effect will be illustrated in Sec 5.1.

The coincidence of the discriminated  $S1$ ,  $S2$ ,  $S3$  signals was delayed to give the common stop to a 17-bit multihit CAEN TDC, with 0.1 ns resolution and 5 ns double edge resolution.

Moreover, another scintillator, about 5 m far from the  $S1$ ,  $S2$ ,  $S3$  cross, was acquired in order to perform a measurement of the particle momentum crossing the setup by means of time of flight. The measured momentum resolution for pion and proton beams in the momentum range between 100 and 440 MeV/c was less than 1%.

In the following, unless otherwise stated, the beam was directed perpendicular to the drift axis of the TPG prototype. The discriminator threshold on the front-end electronics of the TPG signal was set to  $\sim 3.5 \text{ fC}$  and  $\sim 5 \text{ fC}$ .

### 3.1 The readout electronics

The prototype readout is composed by 4 rows of 32 pads for a total of 128 pads. Each pad of  $\sim 3 \times 3 \text{ mm}^2$  was connected to a front-end board based on CARIoca-GEM chip [13]. Such chip was developed for the GEM readout in the LHCb Muon Apparatus and it allows to readout half of a pad row. The discriminated and digitized signals were sent to the 17-bit multihit CAEN TDC. For each electronics channel the leading edge (time hit) and the trailing edge, which allow to measure the Time Over Threshold (TOT) with respect to leading edge, were recorded. This TOT technique has been investigated in order to study the possibility to perform a charge measurement needed for particle identification, taking into account the advantage of a faster data acquisition, pattern



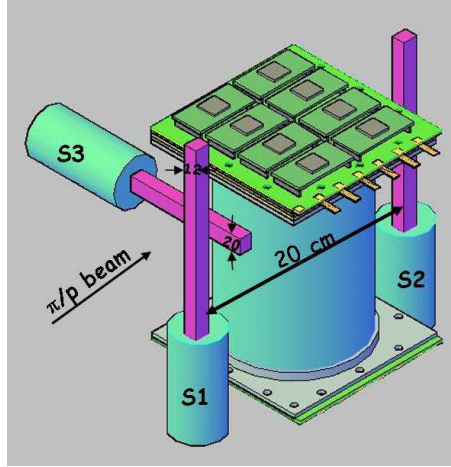


**Figure 7.** Schematic drawing of the experimental setup.

recognition and a better compression into track segment.

#### 4. Gas Mixture Choice

During this R&D phase we decided to use isobutane-based gas mixtures since they are characterized by a large primary ionization (see Sec. 4.1), a high drift velocity (see Sec. 5.1), a high Townsend coefficient, which allow to work at lower HV values (see Sec. 4.2), a moderate longitudinal and transversal diffusions ( $< 400 \mu\text{m}/\sqrt{\text{cm}}$  for a drift field of 150 V) and last but not least a very low attachment coefficient as shown in Fig. 8.

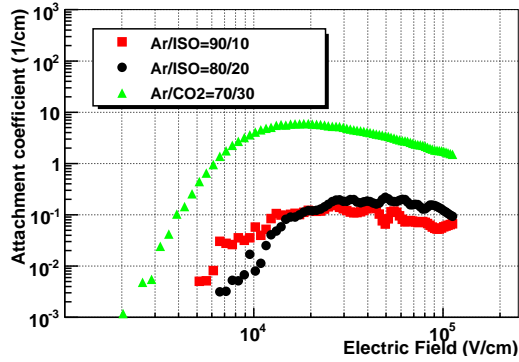


**Figure 8.** Attachment coefficient as a function of the electric field. The curve of the  $\text{Ar}/\text{CO}_2=70/30$  gas mixture is reported for comparison.

##### 4.1 Primary Ionization

The primary ionization of the gas mixtures used during the beam test has been estimated with GARFIELD [15] simulation tool, which is the common framework used for the simulation of gas detectors.



In Tab. 1 have been reported the number of clusters per cm and the number of electrons per cluster for different momentum beam and for the tested gas mixtures. It is worth noticing that the use of isobutane-based gas mixtures allow to reach a larger primary ionization with respect to the Ar/CO<sub>2</sub>=70/30 gas mixture.

Gas Mixture		170 MeV/c	440 MeV/c	MIPs
		Pion	Proton	
Ar/C <sub>4</sub> H <sub>10</sub> 80/20	clu/cm	45.2±2.1	96.6±3.5	40.0±2.0
	e <sup>-</sup> /clu	2.13±0.12	2.12±0.11	2.11±0.11
Ar/C <sub>4</sub> H <sub>10</sub> 90/10	clu/cm	37.2±1.9	79.6±2.8	32.8±1.8
	e <sup>-</sup> /clu	2.14±0.12	2.12±0.11	2.12±0.10
Ar/CO <sub>2</sub> 70/30	clu/cm	32.2±1.8	68.8±2.6	28.4±1.6
	e <sup>-</sup> /clu	2.19±0.13	2.20±0.13	2.21±0.14

**Table 1.** Primary ionization in the tested gas mixture for different particle momentum. The Ar/CO<sub>2</sub>=70/30 gas mixture and MIPs are reported for comparison.

## 4.2 Gas Gain Measurement

The effective gain of a triple-GEM detector has been measured for different gas mixtures using a high intensity 5.9 keV X-ray tube. Effective gain value were obtained from the ratio of pad current with high voltage on the GEM foils, to current on the first GEM, with no high voltage on the GEM foils as shown in Fig. 9. For each gas mixture the detector has been operated with field configurations optimising the electron transparency [14] and the ion feed-back.

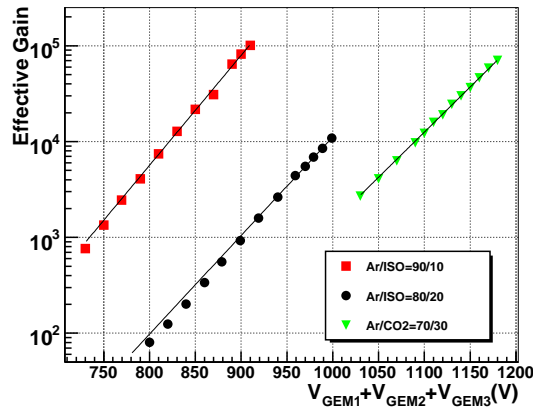


**Figure 9.** Effective gain as a function of the sum of the voltages applied on the three GEM foils for different gas mixture. The curve of the Ar/CO<sub>2</sub>=70/30 gas mixture is reported for comparison.

## 5. Detector Performances

### 5.1 Drift Velocity

The measurement of the drift velocity of the primary electrons in the drift gap for a fixed gas



mixture is needed for the time-space relationship.

For this measurement the beam was shot perpendicular to the field cage. Since it was not possible to measure with great accuracy the distance of the impact point of the beam on the detector field-cage with respect to the upper face of the first GEM, the drift velocity has been calculated as the ratio between the S3 scintillator height ( $20 \pm 1$  mm) and the full width at half maximum of the drift-time distribution. The relative error on the drift velocity is less than  $2 \mu\text{m/ns}$ .

Fig. 10 shows an example of the drift-time distribution. It should be noted that the edge of that distribution is cut by the finite size of the S3 scintillator height.

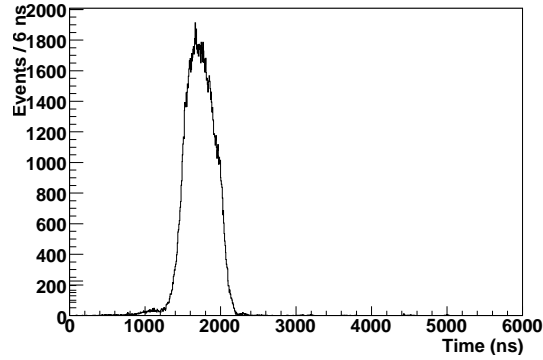


**Figure 10.** Drift-time distribution: Ar/C<sub>4</sub>H<sub>10</sub>= 90/10 gas mixture; Drift Field= 200 V/cm; Gas Gain=  $8 \times 10^3$ .

The drift velocity has been measured for different values of drift field and for the Ar/C<sub>4</sub>H<sub>10</sub>= 90/10 and Ar/C<sub>4</sub>H<sub>10</sub>=80/20 gas mixtures, respectively. The measurements are shown in Fig. 11, along with the corresponding Magboltz prediction [16]. For comparison the drift velocity of the Ar/CO<sub>2</sub>=70/30 is  $3.5 \mu\text{m/ns}$  with a drift field of 150 V/cm.

In the following data analysis, the measured drift velocity has been used for the determination of the z-coordinate of the hits along the axis of the detector.

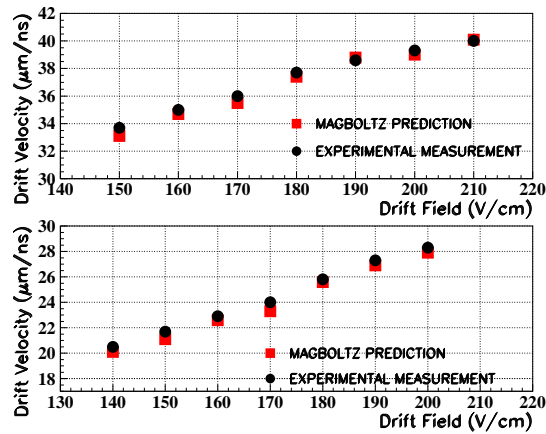


**Figure 11.** Measurements of the electron drift velocity as a function of the drift field. Magboltz predictions are also shown for comparison. Up: for the Ar/C<sub>4</sub>H<sub>10</sub>= 90/10; Bottom: Ar/C<sub>4</sub>H<sub>10</sub>= 80/20.



## 5.2 Efficiency

The single pad row detection efficiency has been evaluated considering the fraction of the hits in a single pad row with respect to a selected track.

An example of the single pad efficiency for the full detector and for each row is shown Fig. 12.

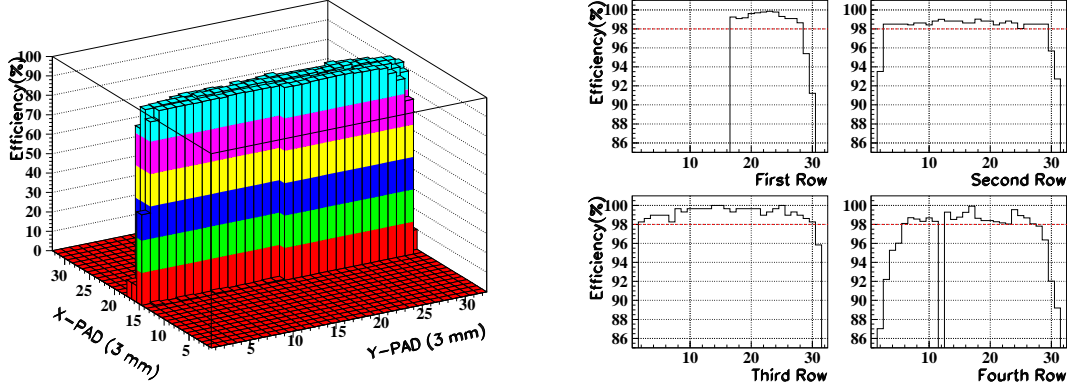


**Figure 12.** Single pad row efficiency for the full detector (left) and for each row (right). Each pad is  $\sim 3 \times 3$  mm<sup>2</sup>.

It is worth noticing that most of the pads have a detection efficiency larger than 98% except for the first 16 channels of the first row and the 11<sup>st</sup> channel of the fourth row that are dead. A low and/or not full detection efficiency in the first and last pads of each rows and a parabolic behaviour are clearly visible.

These effects will be discussed more in detail in Sec. 5.6. Moreover, the first and the fourth rows suffer of a geometrical misalignment of the detector with respect to the trigger system which causes a small loss of hits.

In the following, unless otherwise stated, the first and the last two pads of each row have been not considered in the selection of a track.

In Fig. 13 the detection efficiency for the Ar/C<sub>4</sub>H<sub>10</sub>= 80/20 and Ar/C<sub>4</sub>H<sub>10</sub>= 90/10 gas mixtures as a function of the gas gain with a drift field of 150 V/cm and 170 MeV/c pions is shown. As expected the use of 3.5 fC front-end electronics threshold allows to reach a full efficiency at lower values of gain with respect to the measurements performed with 5 fC of threshold.

The increasing of drift field from 150 V/cm to 210 V/cm with a fixed gain of  $\sim 8 \times 10^3$  allows to increase the detection efficiency from  $\sim 70\%$  to  $\sim 90\%$  for both gas mixtures at 5 fC threshold and from  $\sim 90\%$  to a full efficiency for Ar/C<sub>4</sub>H<sub>10</sub>= 90/10 gas mixture at 3.5 fC threshold as shown in Fig. 14. This effect is due a greater collection efficiency of primary electrons in the first GEM when the drift field is increased.

Moreover, the different level of detection efficiency between the two curves at 5 fC threshold is due to the higher number of primary electrons produced in the drift gap in the Ar/C<sub>4</sub>H<sub>10</sub>= 80/20 gas mixture with respect to the Ar/C<sub>4</sub>H<sub>10</sub>= 90/10 one (see Tab. 1).

In Fig. 15 is shown the detection efficiency for 440 MeV/c proton and 170 MeV/c pion beams crossing the detector. As expected, due to the higher ionization, protons allow to reach an efficiency plateau at lower values of gas gain with respect to pions. The high value of primary ionization



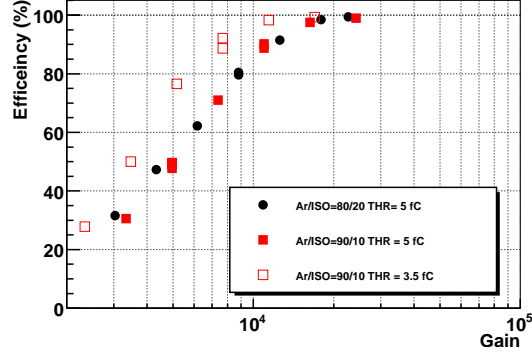


**Figure 13.** Detection Efficiency for the Ar/C<sub>4</sub>H<sub>10</sub>= 80/20 and Ar/C<sub>4</sub>H<sub>10</sub>= 90/10 gas mixtures as a function of the gas gain with a fixed drift field of 150 V/cm and 170 MeV/c pion beam.

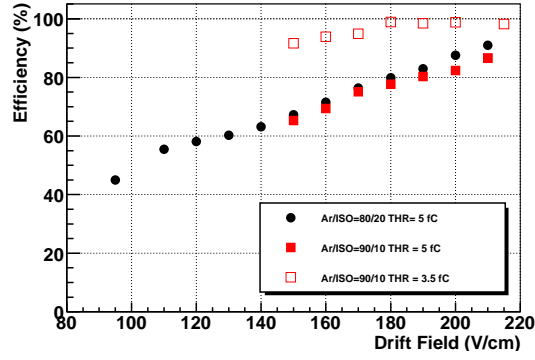


**Figure 14.** Detection Efficiency for the Ar/C<sub>4</sub>H<sub>10</sub>= 80/20 and Ar/C<sub>4</sub>H<sub>10</sub>= 90/10 gas mixtures as a function of drift field with a fixed gain of  $\sim 8 \times 10^3$  and 170 MeV/c pion beam.

obtained with protons does not seem to affect the detection efficiency for the two threshold values, while for pions such effect does not occur, as explained before.

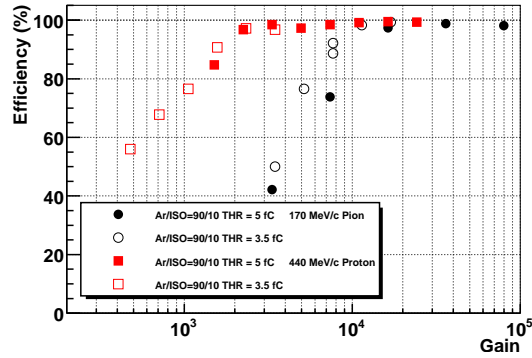
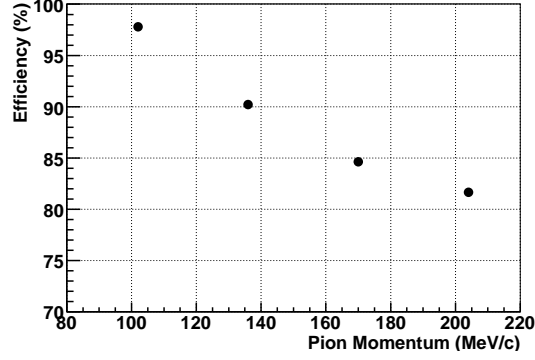


**Figure 15.** Detection Efficiency for protons of 440 MeV/c and pions of 170 MeV/c as a function of the gas gain. The gas mixture is Ar/C<sub>4</sub>H<sub>10</sub>= 90/10 and the drift field is set to 150 V/cm.

The primary ionization effect has been also evaluated measuring the detector efficiency as a



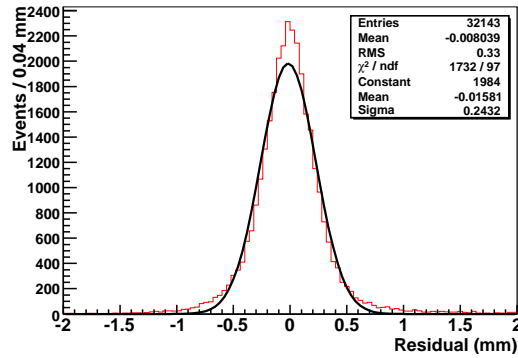
function of the pion beam momentum in the range between 100 and 200 MeV/c (Fig. 16). As expected a higher efficiency value is obtained with a pion momentum of  $\sim 100$  MeV/c.



**Figure 16.** Detection Efficiency as a function of pion momentum in Ar/C<sub>4</sub>H<sub>10</sub>= 80/20 gas mixture. The gain is set to  $\sim 8 \times 10^3$  and the drift field is 190 V/cm.

### 5.3 Spatial Resolution

The spatial resolution in the drift direction was evaluated by the residuals between the hit position in a single pad row and a selected track. The best spatial resolution obtained during the beam test is shown in Fig. 17.



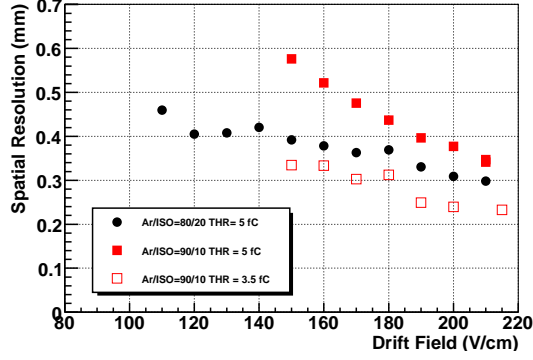
**Figure 17.** The best spatial resolution obtained with 440 MeV/c proton and the Ar/C<sub>4</sub>H<sub>10</sub>= 90/10 gas mixture. The drift field is set to 150 V/cm and the gas gain is  $\sim 5 \times 10^3$ .

Fig. 18 shows the spatial resolution in the drift direction for 170 MeV/c pions as a function of the drift field. Since both the diffusion coefficient decreases and the collection efficiency of primary electrons in the first GEM increases by increasing the drift field, a better spatial resolution is achieved for high drift field and low value of threshold.

Moreover, it should be noted that for 5 fC threshold value a better spatial resolution is reached with Ar/C<sub>4</sub>H<sub>10</sub>= 80/20 with respect to the Ar/C<sub>4</sub>H<sub>10</sub>= 90/10 gas mixture due to a lower diffusion coefficient.

The spatial resolution for 170 MeV/c pions as a function of the gas gain at fixed drift field is shown in Fig. 19. For the 3.5 fC threshold value, the spatial resolution decreases by increasing the





**Figure 18.** Spatial resolution in the drift direction for the  $\text{Ar}/\text{C}_4\text{H}_{10} = 80/20$  and  $\text{Ar}/\text{C}_4\text{H}_{10} = 90/10$  gas mixtures as a function of the drift field with a fixed gain of  $\sim 8 \times 10^3$  and 170 MeV/c pions.

detector gain due to a higher collection efficiency in the first GEM until it reaches a plateau region. On the contrary, for a high value of threshold and for both gas mixtures the spatial resolution seems to be not affected by the detector gain. A possible explanation is that the collection efficiency in the first GEM increases as the detector gain increases until the signal is above the discrimination threshold. When this happens a better spatial resolution is achieved reaching a plateau when the signal is comparable with the electronic threshold.

Such explanation is confirmed by the fact that at very low gains ( $< 3 \times 10^3$ ), the  $\text{Ar}/\text{C}_4\text{H}_{10} = 90/10$  gas mixture reaches the same value of spatial resolution regardless of the used threshold.

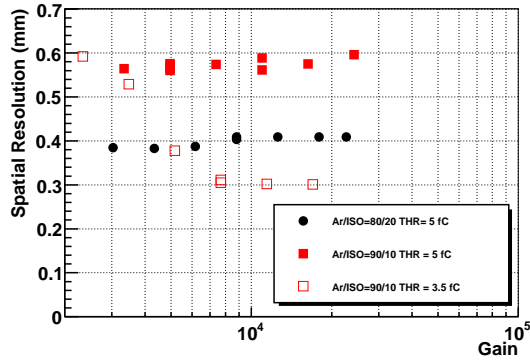


**Figure 19.** Spatial resolution in the drift direction for the  $\text{Ar}/\text{C}_4\text{H}_{10} = 80/20$  and  $\text{Ar}/\text{C}_4\text{H}_{10} = 90/10$  gas mixtures as a function of gas gain with a fixed drift field of 150 V/cm and 170 MeV/c pions.

The effect of the ionizing particle on the spatial resolution has been evaluated comparing 440 MeV/c proton with 170 MeV/c pion as shown in Fig. 20. As explained above, the spatial resolution seems not so sensible to a gain change with 5 fC threshold value and regardless of ionization particle. Moreover, the larger ionization produced by protons with respect to pions allows to reach a better spatial resolution of about a factor 2.

At 3.5 fC of threshold, the spatial resolution for pions reaches at high gain the same level obtained with protons. This indicates that, together with the fact that there are no differences in the measurement of spatial resolutions with protons at different threshold values, the spatial



resolution has reached a limit value for the  $\text{Ar}/\text{C}_4\text{H}_{10} = 90/10$  gas mixture.

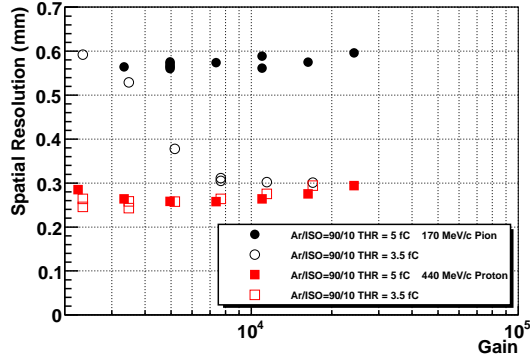


**Figure 20.** Spatial resolution for proton of 440 MeV/c and pion of 170 MeV/c as a function of the gas gain. The gas mixture is  $\text{Ar}/\text{C}_4\text{H}_{10} = 90/10$  and the drift field is set to 150 V/cm.

Fig. 21 shows the spatial resolution as a function of pion beam momentum in the range between 100 MeV/c and 200 MeV/c. As expected, the spatial resolution results to be effected by low value of pion momentum.

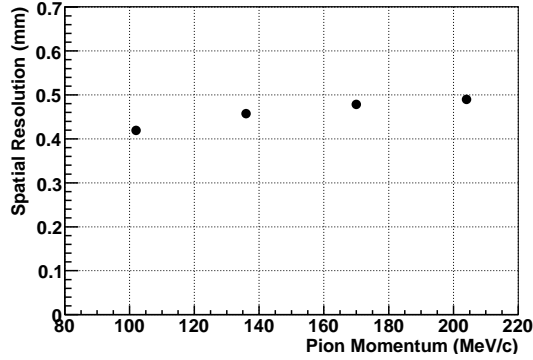


**Figure 21.** Spatial resolution as a function of pion momentum in  $\text{Ar}/\text{C}_4\text{H}_{10} = 80/20$  gas mixture. The gain is set to  $\sim 8 \times 10^3$  and the drift field is 190 V/cm.

#### 5.4 Time Over Threshold measurement

Timing functionality in the CARIOCA-GEM chip allows also the measurement of charge, and therefore of ionization, for individual channels. The measurement of signal pulse width above a preset discriminator threshold may be used to a good approximation as a determination of the charge on each channel. From the collection of all channel measurements the track ionization can be well determined. As a confirmation of the ability of the CARIOCA-GEM chip to measure simultaneously timing and ionization, the charge density along tracks has been determined using the Time Over Threshold (TOT) measurement as shown in Fig. 22.

It should be noted that the distribution of Fig. 22 follows a Landau distribution as expected. Moreover, the analysis has shown that this distribution is essentially independent of the track orientation.



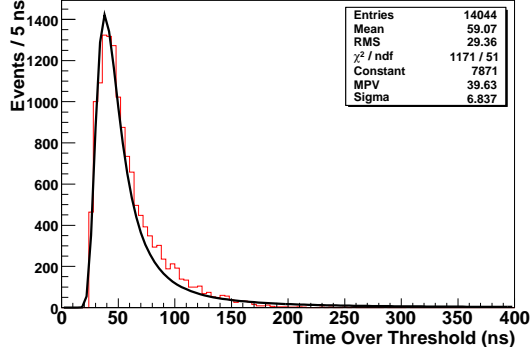


**Figure 22.** Distribution of the Time Over Threshold (TOT) measurements along tracks with a 100 MeV/c pion beam. The TOT distribution has been fitted with a Landau distribution.

### 5.5 Particle Identification using dE/dx

Energy loss, dE/dx, were measured for pions and protons to evaluated the PID capability of our TPG prototype.

The dE/dx resolution was measured using the truncated technique. We observe that by accepting the 40% lowest dE/dx values of the hits in the track we obtain the best resolution and we correctly reproduce the most probable value of the single pad charge distribution. For higher values of the accepted fraction, the resolution gets worse due to inclusion of hits from the Landau distribution tail, while for smaller values the effect is related to the loss in statistics.

Fig. 23 shows the Gaussian behaviour of the resulting distribution when a cut of 60% is applied.

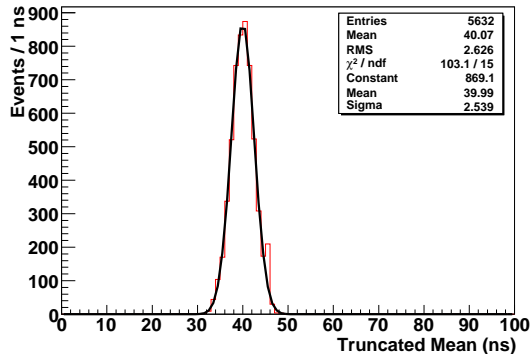


**Figure 23.** Truncated mean distribution in a sample of 30 hits obtained by removing the 60% largest signals with a 100 MeV/c pion beam.

By simultaneously measuring the momentum for proton and pion beams, by means of the time of flight (see Sec. 3), and the deposited energy, by means of the mean value of the truncated distribution, an estimation of the TPG prototype ability to identify the particle crossing the detector can be performed as shown in Fig. 24.

For a fixed particle momentum, the dE/dx resolution function is usually parametrized [17] as:

$$\sigma_{dE/dx} \propto N^a x^b \quad (5.1)$$



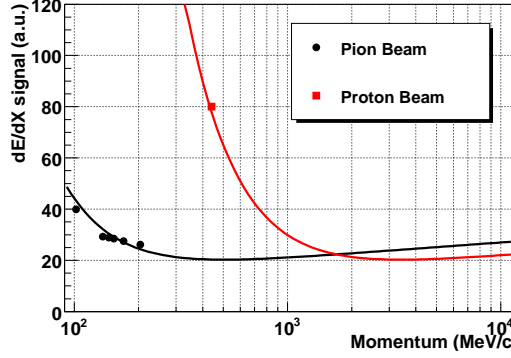


**Figure 24.** Measured  $dE/dx$  signal as a function of the momentum for pion and proton beams with the  $\text{Ar}/\text{C}_4\text{H}_{10} = 80/20$  gas mixture. The gain is set to  $\sim 8 \times 10^3$  and the drift field is 190 V/cm.

where  $N$  the number of samples and  $x$  their length which in our case is the pad dimension (Fig. 25). In the used  $\text{Ar}/\text{C}_4\text{H}_{10} = 80/20$  gas mixture at atmospheric pressure, we measured  $a = -0.40 \pm 0.02$  and  $b = -0.26 \pm 0.05$ .

Assuming an average track length corresponding to 100 hits in the TPG-AMADEUS, with 100 MeV/c pion and 40% of accepted fraction, we expect to measure a  $dE/dx$  resolution of about 9%. This energy resolution is comparable with that obtained with STAR TPC with a track length of more than 67 cm [18].

Moreover we expect to achieve, with such energy resolution and with a 100 MeV/c particle momentum, a  $K/\pi$  and  $\pi/p$  separation power of 75 and 260, respectively.

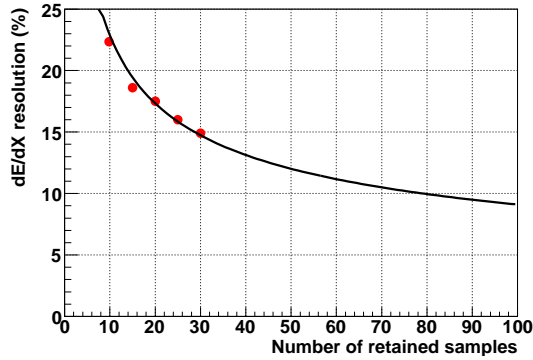


**Figure 25.**  $dE/dx$  resolution as function of the number of used hits with a truncated mean cut of 60%. The curve is the expected  $dE/dx$  resolution.

## 5.6 Edge Effect due to the Field Cage

Low and/or not full detection efficiency has been measured on the edge of each pad rows as clearly visible in Fig. 12.

Such effects are due to different reasons:



- the length of each pad row is 102 mm while the effective diameter of the cylindrical field-cage is 100 mm. This means that the first and the last pad of each row collect about 2/3 of the charge with respect to the other pads of the row (Fig. 26);
- electric distortion of the field in the drift gap mainly near the field-cage are not completely cured;
- the primary electrons produced in the drift gas and drifting toward the first GEM can be collected by the internal strips of the field-cage (Fig. 27).

In any case all these effects are fully reduced drifting away from the field-cage by  $\sim 5$  mm.

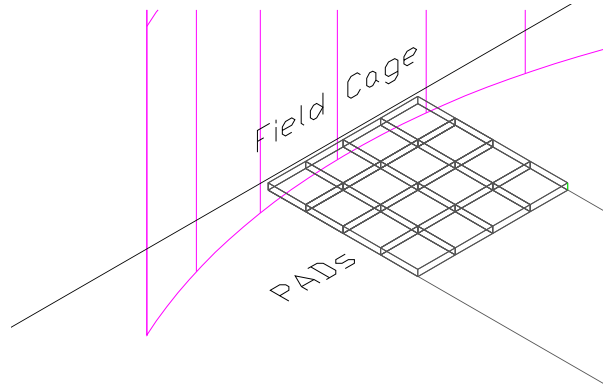


**Figure 26.** Drawing of the readout pads with the field cage wall.

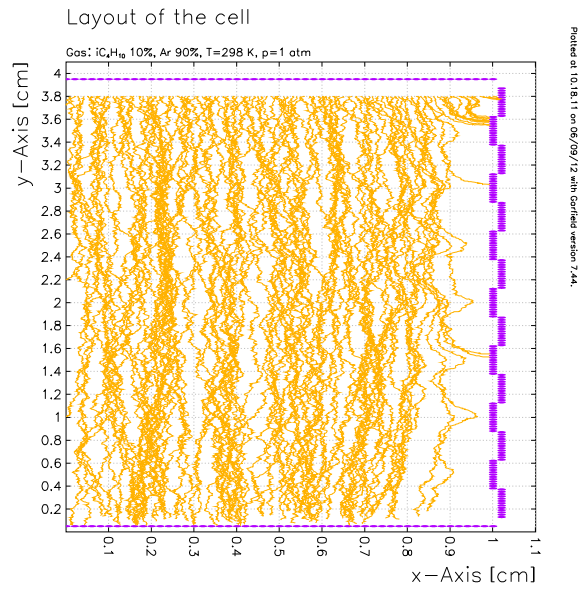


**Figure 27.** Garfield simulation of primary electrons in the drift gap.



## 6. Conclusion

The R&D activity on TPG detector for the inner part of the AMADEUS experiment has started at Laboratori Nazionali di Frascati (INFN). A TPG prototype, with a drift gap up to 15 cm, has been successfully produced and tested at the  $\pi$ M1 beam facility of the Paul Scherrer Institut with low momentum pion and proton beams.

The drift properties of various argon-isobutane gas mixtures have been measured and they result compatible with those simulated with Magboltz.

The measurement of the detector performances, in terms of detection efficiency and spatial resolution, as a function of the gas gain, drift field, front-end electronics threshold and particle momentum has been reported and discussed in detail. A detection efficiency of 99% and a resolution along the drift direction of 240  $\mu$ m have been achieved.

The dE/dx resolution has been measured for isobutane-based gas mixture applying a truncated mean of 60%. A good energy resolution, of about 25% on a single measurement, will allow to reach an overall resolution of about 8% for an average track length in AMADEUS-TPC.

Finally, the effect of the field-cage on the detector performances has been also measured showing that it is necessary to move about 5 mm away from the field-cage.

## Acknowledgments

The authors would like to thank the coordinator of the PSI beam lines, Dr. Konrad Deiters, for the excellent cooperation and support; M. Pistilli for his suggestions during the prototype design phase and for his highly qualified technical assistance during its assembly.

Part of this work was supported by the European Community-Research Infrastructure Integrating Activity “Study of Strongly Interacting Matter” HadronPhysics 2 (HP2), Grant Agreement No. 227431, and HadronPhysics 3 (HP3), Contract No. 283286, under the Seventh Framework Programme of EU.

## References

- [1] AMADEUS Collaboration, *AMADEUS Letter of Intent*.
- [2] AMADEUS Collaboration, *AMADEUS Phase-1: Setup and Roll-in Proposal*, **LNF-07/24(IR)** 2007.
- [3] D. Adinolfi et al., *Nucl. Instr. and Meth.* **A 461** (2001) 25.
- [4] D. Alesini et al., *DAFNE upgrade for SIDDHARTA RUN*, **LNF-06/33(IR)** 2006.
- [5] C. Milardi, *DAΦNE Interaction Regions Upgrade*.
- [6] M. Bazzi et al., *Nucl. Instr. and Meth.* **A 671** (2012) 125.
- [7] F. Sauli, *Nucl. Instr. and Meth.* **A 386** (1997) 531.
- [8] M. Alfonsi et al., *Nucl. Instr. and Meth.* **A 518** (2004) 106.
- [9] M. Poli Lener, *Triple-GEM detectors for the innermost region of the muon apparatus at the LHCb experiment*, *Ph.D Thesis*, **CERN-THESIS-2006-13**.
- [10] F. Sauli et al., *Nucl. Instr. and Meth.* **A 560** (2006) 269, **CERN-PH-EP/2005-056**.



- [11] P. de Simone et al., *IEEE Trans. Nucl. Sci.* **52** (2005) 2872.
- [12] G. Bencivenni et al., *Nucl. Instr. and Meth.* **A 572** (2007) 168.
- [13] M. Poli Lener et al., *IEEE NSS MIC* **Vol. 6** (2007) 4671.
- [14] G. Bencivenni et al., *Nucl. Instr. and Meth.* **A 488** (2002) 493.
- [15] R. Veenhof, *Nucl. Instr. and Meth.* **A 419** (1998) 726.
- [16] S.F. Biagi, *Nucl. Instr. and Meth.* **A 412** (1999) 234.
- [17] W. Allison, J.H. Cobb., *Ann. Rev. Nucl. Part. Sci* **30** (1980) 253.
- [18] M. Anderson et al., *Nucl. Instr. and Meth.* **A 499** (2003) 569.